J Biomol NMR (2011) 50:277–284
DOI 10.1007/s10858-011-9516-2

ARTICLE

Chemical shift correlation at high MAS frequencies employing low-power symmetry-based mixing schemes

Christian Herbst · Jirada Herbst · Jörg Leppert · Oliver Ohlenschläger · Matthias Görlach · Ramadurai Ramachandran

Received: 1 March 2011 / Accepted: 11 May 2011 / Published online: 11 June 2011

Abstract An approach for conveniently implementing low-power CN_n^v and RN_n^v symmetry-based band-selective mixing sequences for generating homo- and heteronuclear chemical shift correlation NMR spectra of low γ nuclei in biological solids is demonstrated. Efficient magnetisation transfer characteristics are achieved by selecting appropriate symmetries requiring the application of basic RF elements of relatively long duration and numerically tailoring the RF field modulation profile of the basic element. The efficacy of the approach is experimentally shown by the acquisition of ^{15}N–^{13}C dipolar and ^{13}C–^{13}C scalar and dipolar coupling mediated chemical shift correlation spectra at representative MAS frequencies.

Keywords Solid-state NMR spectroscopy · ^{15}N–^{13}C and ^{13}C–^{13}C dipolar recoupling · ^{13}C–^{13}C scalar recoupling · Symmetry-based pulse sequences

Electronic supplementary material The online version of this article (doi:10.1007/s10858-011-9516-2) contains supplementary material, which is available to authorized users.

J. Leppert · O. Ohlenschläger · M. Görlach · R. Ramachandran (✉)
Research group Biomolecular NMR spectroscopy, Leibniz Institute for Age Research, Fritz Lipmann Institute, 07745 Jena, Germany
e-mail: raman@fli-leibniz.de

C. Herbst (✉)
Department of Physics; Faculty of Science, Ubon Ratchathani University, Ubon Ratchathani 34190, Thailand
e-mail: cherbst@fli-leibniz.de

J. Herbst
Department of Mathematics, Statistics and Computer, Faculty of Science, Ubon Ratchathani University, Ubon Ratchathani 34190, Thailand

In MAS solid state NMR based studies of biomolecular systems such as proteins and RNAs, multi-dimensional experiments involving the application of RF pulse sequences with mixing periods leading to ^{15}N–^{13}C and ^{13}C–^{13}C magnetisation transfers are often carried out for the assignment of resonances and for the extraction of structural constraints (Sun et al. 1997; Baldus et al. 1998; Hong 1999; Rienstra et al. 2000; Pauli et al. 2001; Detken et al. 2001; Castellani et al. 2003; van Rossum et al. 2003; Riedel et al. 2005; Frericks et al. 2006; Siemer et al. 2006; Chen et al. 2006, 2007a, b; Kehlet et al. 2007; Hansen et al. 2007; Zhou et al. 2007a, b; Nielsen et al. 2009, 2011). In a variety of experimental circumstances it is advantageous to employ low-power band-selective mixing sequences. When the mixing sequence has to be applied over a long period, as in the generation of ^{13}C–^{13}C scalar coupling mediated TOBSY correlation spectra (Baldus and Meier 1996) of aliphatic carbons in peptides and proteins, low RF field strength requirements can be very useful for minimising not only the interference between the decoupling and recoupling RF fields (Bennett et al. 1998) but also sample heating effects in temperature sensitive samples. Band-selective mixing sequences can also permit the generation of correlation data with improved cross-peak intensities by reducing the leakage of magnetisation through multiple magnetisation transfer pathways (Rienstra et al. 2000). For example, the use of a broadband ^{15}N–^{13}C mixing sequence in the 3D NCC experiment (Sun et al. 1997; Rienstra et al. 2000) could lead to the transfer of the initial ^{15}N magnetisation to both the $^{13}C^{\alpha}$ and $^{13}C'$ nuclei in proteins. Compared to the experiment in which these intra- and inter-residue correlations are obtained in two separate measurements, by restricting the ^{15}N magnetisation transfer either to $^{13}C^{\alpha}$ or $^{13}C'$ employing band-selective mixing sequences, the cross-peak intensities seen in the broadband experiment are

reduced by a factor of 2. Hence, when sensitivity is critical, it will be clearly advantageous to employ band-selective mixing sequences (Rienstra et al. 2000). Such sequences could also potentially permit the generation of correlation spectra with improved spectral resolution by reducing the spectral width requirements in the indirect dimensions. The need for efficient band-selective mixing schemes for achieving $^{13}C^{\alpha} \rightarrow {}^{15}N$ and $^{13}CO \rightarrow {}^{15}N$ magnetisation transfers can also be seen from the recent studies of Zhou et al. who employed 3D CANH, CONH and CON(H)H type of experiments for achieving ^{1}H resonance assignments and for obtaining ^{1}H–^{1}H distance constraints in their structural study of the $\beta 1$ immunoglobulin binding domain of protein G (GB1) (Zhou et al. 2007a, b). Band-selective mixing sequences are also expected to be useful in the study of RNAs when magnetisation transfers within either the aromatic or sugar moieties are required. It is apparent that an efficient general approach enabling the design of low-power band-selective mixing sequences would have a considerable impact in the structural studies of biomolecular systems. In this context we have examined the potential of the symmetry-based approach (Levitt 2002) for implementing band-selective ^{15}N–^{13}C and ^{13}C–^{13}C mixing sequences at high MAS frequencies that are typically employed in the study of biological systems, e.g. to minimise the effects of CSA at high Zeeman field strengths. One of the strengths of the symmetry-based approach for the recoupling and decoupling of different nuclear spin interactions in rotating solids is that it provides a large number of inequivalent symmetries involving the application of basic "*R*"/"*C*" elements of different durations. Recently, we have developed a numerical approach for the design of broadband mixing sequences using symmetries involving the application of basic elements of short durations (Herbst et al. 2009a, b, c; Herbst 2010; Herbst et al. 2010). For example, symmetries such as $R18_{17}^{-4,\ 5}$ and $R24_{22}^{-5,\ 7}$ requiring basic *R* elements of duration $\sim$63 and 61 μs, respectively, were employed at a MAS frequency of 15 kHz for achieving ^{13}C–^{15}N double-quantum dipolar recoupling (Herbst et al. 2010). By exploiting the fact that 180° and 360° pulses of relatively long duration and with small inversion/null-rotation bandwidths can be implemented using low RF field strengths, the possibility to generate homo- and heteronuclear correlation spectra at high MAS frequencies using low-power band-selective symmtery-based mixing sequences is demonstrated here.

All optimisation calculations were carried out considering simultaneous application of ^{1}H decoupling during mixing. Dual channel ^{15}N–^{13}C mixing sequences leading to γ-encoded heteronuclear double-quantum dipolar recoupling, with suppression of chemical shift anisotropies and homonuclear dipolar coupling terms, were implemented via $RN_n^{\nu_s,\nu_k}$ symmetries (Brinkmann and Levitt 2001; Herbst et al. 2010). TOBSY mixing sequences for achieving efficient ^{13}C–^{13}C magnetisation transfers solely in the spectral range of the aliphatic carbons, as in liquid state NMR, were designed via CN_n^{ν} symmetry-based schemes (Levitt 2002; Hardy et al. 2003; Herbst et al. 2009b). As with TOBSY, mixing sequences for achieving γ-encoded ^{13}C–^{13}C double-quantum dipolar recoupling were also designed via CN_n^{ν} symmetry-based schemes (Levitt 2002; Herbst et al. 2009b). The phase modulated basic *C* and *R* elements of constant amplitude were implemented as a sandwich of a small number of pulses of equal duration. As in our recent studies (Herbst et al. 2009a, b, c; Herbst et al. 2010, Herbst 2010), the global optimisation procedure "genetic algorithms" (GA) was employed to generate the basic *R*/*C* pulses. Subsequently, the phase modulation profiles were tailored numerically via the nonlinear least-squares optimisation procedure NL2SOL implemented in the SPINEVOLUTION program (Veshtort and Griffin 2006), so as to achieve satisfactory performance of the mixing sequence over the required resonance offset range of the nuclei. Band-selective and/or non-band-selective pulses were employed as the starting basic elements in these calculations. A few representative symmetries were considered in the numerical design for which the starting basic elements of the required duration could be constructed with RF field strength in the range of 10–20 kHz. This typically leads to symmetries involving the application of basic elements of relatively long duration. For example, symmetries such as $R16_{49}^{-5,4}$ and $R16_{63}^{-4,5}$ requiring basic *R* elements of duration of $\sim$200 μs were employed at MAS frequencies of 15 and 20 kHz, respectively, for achieving ^{13}C–^{15}N double-quantum dipolar recoupling using ^{15}N and ^{13}C RF field strengths of $\sim$10 kHz. The $C9_{120}^{1}$ and $C9_{69}^{1}$ symmetries involving basic elements of duration $\sim$400 μs were, respectively, used at MAS frequencies of 33.333 and 20 kHz for generating TOBSY mixing sequences using a ^{13}C RF field strength of $\sim$15 kHz. At the MAS frequencies of 25 and 33.333 kHz, the symmetries $C7_{30}^{6}$ and $C7_{40}^{1}$ were, respectively, used for generating ^{13}C–^{13}C dipolar coupling mediated chemical shift correlation spectra using ^{13}C RF field strengths of 15 kHz and 20 kHz. For each of the symmetries considered, the optimisation calculations to find the best possible solution were typically carried out starting with a variety of basic elements, corresponding to RF pulses with different inversion/null rotation bandwidths and phase-modulation profile characteristics.

A Zeeman field strength corresponding to a ^{1}H resonance frequency of 500 MHz and typical chemical shift and dipolar coupling parameters, as indicated in the figure captions, were used in the numerical design. Either a two spin ^{15}N–^{13}C or ^{13}C–^{13}C spin system was employed and

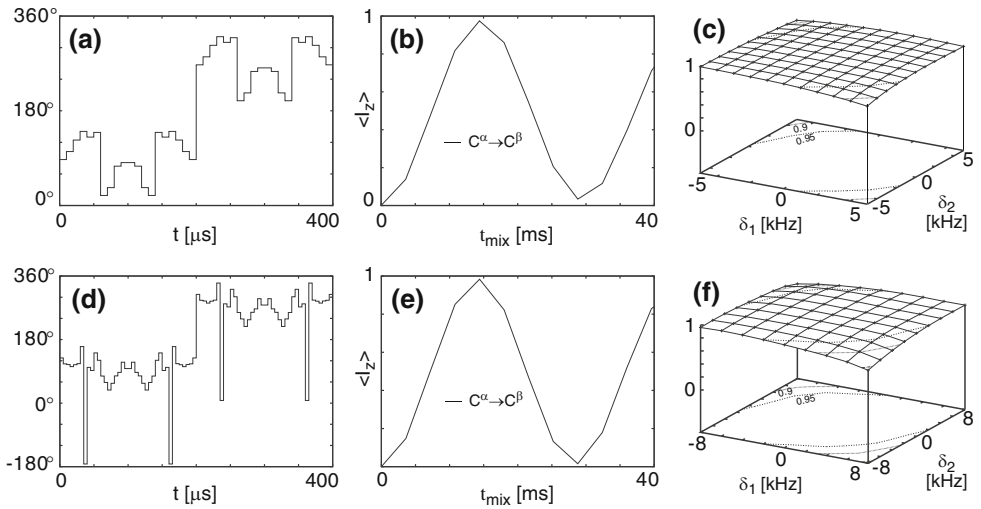

Fig. 1 Simulated longitudinal TOBSY magnetisation transfer characteristics observed with the $C9^{1}_{120}$ symmetry-based RF pulse scheme. The optimised phase-modulation profile of the basic *C* element of 400 μs duration shown in **a** was generated considering an RF field strength of 15 kHz, a spinning speed of 33.333 kHz and a resonance offset range of ± 5 kHz. The simulated plot given in **b** shows the magnitude of the transferred magnetisation (normalised to the maximum transferable signal) on the second carbon starting with *z* magnetisation on carbon 1. These were generated using typical chemical shift, scalar and dipolar coupling parameters of alanine, with the ^{13}C carrier kept at the center of the two resonances. **c** shows the magnitude of the transferred magnetisation on spin 2 at a τ_{mix} of 14.4 ms as a function of the resonance offsets of the scalar coupled nuclei, starting with *z* magnetisation on the first carbon spin at zero mixing time. The corresponding optimised phase-modulation profile of the basic element and the performance characteristics of the sequence obtained considering a resonance offset range of ±8 kHz and an RF field strength of 20 kHz are given in the plots shown in **d**–**f**. The RF phase values of the first 10 slices of the basic C element are given in the supplementary material

optimised RF pulse schemes were obtained, as in our recent studies, by monitoring the transfer of longitudinal magnetisation to the second spin, starting with *z* magnetisation on spin 1 at zero mixing time, and maximising the magnitude of the longitudinal magnetisation at different mixing times (^{15}N–^{13}C mixing: ∼3 ms, ^{13}C–^{13}C double-quantum dipolar mixing: ∼1.2 ms, TOBSY mixing: ∼14 ms). In the case of TOBSY, efficient mixing sequences could be generated by first obtaining the optimised liquid state TOCSY mixing sequences using the relevant CN^{ν}_{n} symmetry-based RF phasing scheme. The resultant phase-modulation profile was then subsequently used as the starting point for obtaining the TOBSY mixing sequence.

In general, the local optimisation calculations were repeated several times varying all the RF phase values randomly over a range of ±10%. These calculations were carried out employing a variety of computer systems including a unix cluster with 64 processors, incorporating RF field inhomogeneities (±5%) and considering only a limited number of 32 crystallite orientations selected according to the Zaremba-Cheng-Wolfsberg (ZCW) method (Cheng et al. 1973). All simulations to assess the performance characteristics of the pulse sequences were carried out with the SPINEVOLUTION program (Veshtort and Griffin 2006) considering 168 α and β powder angles selected according to the REPULSION scheme (Bak and Nielsen 1997) and 16 γ angles as well as with a Zeeman field strength corresponding to a ^{1}H resonance frequency of 500 MHz. Chemical shift correlation experiments via longitudinal magnetisation exchange were carried out as in our earlier studies using polycrystalline (^{13}C,^{15}N) labelled samples of arginine and the CUG triplet repeat expansion RNA $(CUG)_{97}$ (Riedel et al. 2005, 2006; Herbst et al. 2010; Herbst 2010) in a Bruker 500 MHz wide-bore or a narrow-bore Bruker 750 MHZ Avance III solid state NMR spectrometer equipped with 3.2 and 2.5 mm triple resonance probes, with the sample temperature kept at ∼0°C. Other details are given in the figure captions.

Phase-modulated 180° and 360° pulses with the required duration were generated via GA considering inversion/null-rotation bandwidths in the range of 2–20 kHz and appropriate RF field strengths, as mentioned earlier. 180° pulses were generally constructed such that the phase modulation profile is symmetric with respect to the center of the pulse. The null rotation pulses were generated such that the phase modulation profile of the first half of the pulse is 180° out of phase with respect to the second half and, additionally, the phase-modulation profile of each half was kept symmetric with respect to its center. As representative examples, the phase- modulation profiles and the performance characteristics of some of the GA derived pulses are given in the supplementary material. Starting with a variety of basic *C* elements, TOBSY optimisation calculations were carried out considering a resonance offset range of ±5 kHz

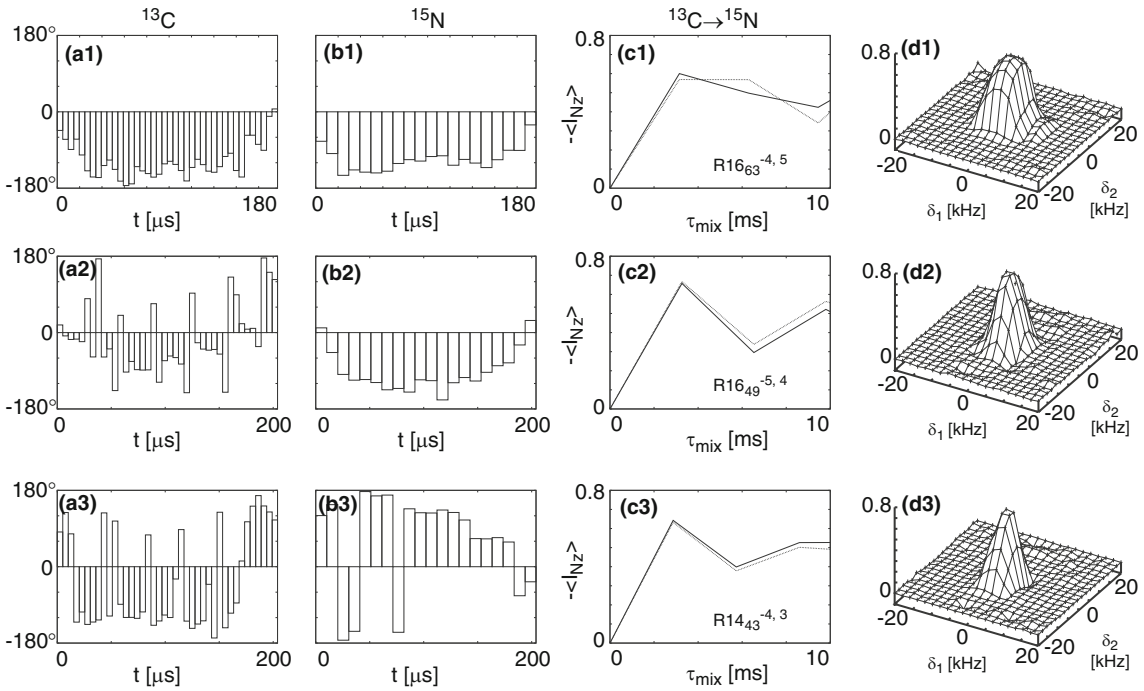

Fig. 2 Phase-modulation profiles (ai,bi)$_{i=1-3}$ and simulated ^{13}C·^{15}N magnetisation transfer characteristics (ci,di)$_{i=1-3}$ of the numerically optimised symmetries R16$_{63}^{-4,5}$ (**a1**, **b1**, **c1**, **d1**; 20 kHz), R16$_{49}^{-5,4}$(**a2**, **b2**, **c2**, **d2**; 15 kHz) and R14$_{43}^{-4,3}$ (**a3**, **b3**, **c3**, **d3**; 15 kHz). The optimised phase-modulation profiles were generated considering a resonance offset range of ±2 kHz and ^{13}C and ^{15}N RF field strengths of 10 kHz. The simulated plots (**c1**–**c3**) show the magnitude of the transferred magnetisation (normalised to the maximum transferable signal) on nitrogen starting with z magnetisation on carbon (continuous lines $^{13}C^{\alpha} \rightarrow {}^{15}$N and dotted lines $^{13}C' \rightarrow {}^{15}$N). The simulations were carried out using appropriate chemical shift, scalar and dipolar coupling parameters as in our recent study (Herbst et al. 2010). Plots given in (**d1**–**d3**) show, respectively, the magnitude of the transferred magnetisation on nitrogen at a τ_{mix} of 3.15, 3.27 and 2.87 ms as a function of the resonance offsets of the dipolar coupled nuclei, starting with z magnetisation on the carbon ($^{13}C'$) spin at zero mixing time. The RF phase values of the slices of the basic R elements as well as the zoomed plots of (**d1**–**d3**) are given in the supplementary material

and an RF field strength of 15 kHz. The phase-modulation profile of the optimised basic C element for the $C9_{120}^{1}$ symmetry at a MAS frequency of 33.333 kHz is given in Fig. 1a. It was obtained by first generating the optimised liquid state TOCSY mixing sequences using the $C9_{120}^{1}$ symmetry-based RF phasing scheme and employing the resultant phase-modulation profile as the starting point for obtaining the TOBSY mixing sequence. CSA, scalar and dipolar coupling parameters corresponding to that of the $^{13}C^{\alpha}$ and $^{13}C^{\beta}$ nuclei of alanine were used in the TOBSY calculations and the ^{13}C carrier was kept at the middle of the aliphatic spectral region. The simulated magnetisation transfer characteristics given in Fig. 1b indicate that the $C9_{120}^{1}$ symmetry can be effectively employed for generating TOBSY spectra in the aliphatic region of peptides and proteins. Figure 1c shows the magnitude of the transferred magnetisation on spin 2 at a τ_{mix} of ~14 ms as a function of the resonance offsets of the scalar coupled nuclei, starting with z magnetisation on the first carbon spin at zero mixing time. It is apparent that the performance of the sequence is not very much dependent on the resonance offsets of the two nuclei in the offset range considered. At the MAS frequency of 33.333 kHz, TOBSY optimisation calculations were also carried out employing a resonance offset range of ±8 kHz and an RF field strength of 20 kHz. The corresponding optimised phase-modulation profile of the basic element and the performance characteristics of the sequence are given in the plots shown in Fig. 1d–f. Such mixing sequences are expected to be useful for carrying out band-selective TOBSY experiments at very high Zeeman field strengths. Optimised low-power TOBSY mixing sequences derived considering other experimental conditions are given in the supplementary material. Although the TOBSY mixing sequences reported here were obtained without imposing any restriction for minimising the transfer outside the aliphatic spectral window, negligible $^{13}C^{\alpha} \rightarrow {}^{13}C'$ transfer is typically seen with all the mixing sequences. Where needed mixing sequences can be designed including a penalty term for further minimising magnetisation transfer outside the bandwidth of interest, albeit at the cost of more computational time.

Typical CSA parameters in the ^{15}N channel and nominal as well as large ^{13}C CSA values were considered in the numerical optimisation runs for generating low-power

band- selective $RN_n^{\nu_s,\nu_k}$ symmetry-based dual channel RF pulse schemes for γ-encoded ^{15}N–^{13}C dipolar recoupling. The simulated performance characteristics of some of the $RN_n^{\nu_s,\nu_k}$ symmetry-based sequences are shown in Fig. 2 along with the optimised RF field-modulation profiles of the basic elements. The optimised profiles $(ai, bi)_{i\,=\,1-3}$ were obtained considering a resonance offset range of (±2 kHz, ±2 kHz) and RF field strength of 10 kHz for the $^{13}C'$ and ^{15}N nuclei, without restricting the phase modulation profile to be symmetric with respect to the center of the pulse. The simulated plots c1–c3 show the magnitude of the transferred magnetisation (normalised to the maximum transferable signal) on nitrogen starting with z magnetisation on carbon at zero mixing time. Plots given in Fig. 2 d1–d3 show the magnitude of the transferred magnetisation on nitrogen at τ_{mix} of 3.15, 3.27 and 2.87 ms, respectively, as a function of the resonance offsets of the dipolar coupled nuclei. The performance of the numerically optimised symmetry-based schemes reported here were in general found to be not affected by minor variations (±5%) in the RF field strength employed (data not shown) as well as by considering smaller ^{13}C CSA values. Recoupling sequences could also be successfully designed considering marginally larger resonance offset ranges for the ^{13}C nuclei, as will be required in $^{13}C^{\alpha} \rightarrow {}^{15}N$ transfers. A representative plot of the optimised phase-modulation profiles and the simulated $^{13}C^{\alpha} \rightarrow {}^{15}N$ magnetisation transfer characteristics generated with the $R16_{63}^{-4,5}$ symmetry considering a resonance offset range of ±3 kHz and ±2 kHz, respectively, in the ^{13}C and ^{15}N dimensions are given in the supplementary material. From the numerical simulation results shown in Fig. 2, it can be seen that by choosing appropriate symmetries it is possible to implement efficient band-selective ^{13}C–^{15}N dipolar recoupling schemes even at high MAS frequencies using only a moderate $^{13}C/^{15}N$ RF field strength in the range of 10 kHz. The mixing sequences reported here were generated without imposing any restriction for minimising the transfer outside the $^{15}N/^{13}C$ spectral window of interest. However, with the ^{13}C carrier kept at the carbonyl region, sequences designed for efficient $^{15}N \leftrightarrow {}^{13}C'$ magnetisation transfer show minimal $^{15}N \leftrightarrow {}^{13}C^{\alpha}$ transfers. Similarly, with the carbon carrier kept at the $^{13}C^{\alpha}$ region, mixing sequences designed for efficient $^{15}N \leftrightarrow {}^{13}C^{\alpha}$ magnetisation transfer show minimal $^{15}N \leftrightarrow {}^{13}C'$ transfers. It is worth noting that although the mixing sequences reported here were designed considering a particular MAS frequency, it is possible to realise satisfactory magnetisation transfer characteristics (over the correspondingly scaled spectral range) at other MAS frequencies by appropriate scaling of the duration of the optimised basic element and RF field strength.

Considering a resonance offset range of ±5 kHz, calculations were carried out for achieving band-selective ^{13}C–^{13}C double-quantum dipolar recoupling via the $C7_{30}^{6}$

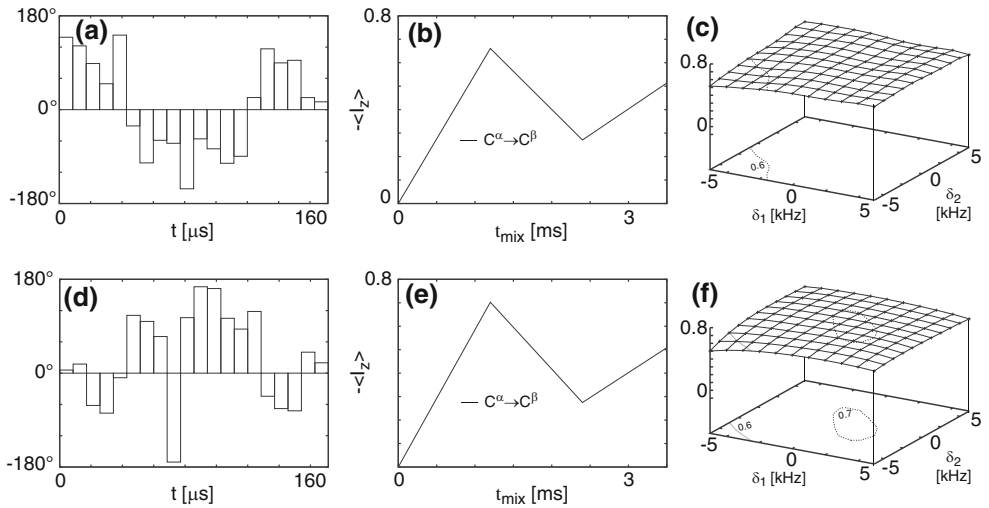

Fig. 3 Simulated longitudinal dipolar magnetisation transfer characteristics observed with the $C7_{30}^{6}$ symmetry-based RF pulse scheme. The optimised phase-modulation profile of the basic C element of ~171 μs duration shown in **a** was generated considering an RF field strength of 15 kHz, a spinning speed of 25 kHz and a resonance offset range of ±5 kHz. The simulated plot given in **b** shows the magnitude of the transferred magnetisation (normalised to the maximum transferable signal) on the second carbon starting with z magnetisation on carbon 1. These were generated using typical chemical shift, scalar and dipolar coupling parameters of alanine, with the ^{13}C carrier kept at the center of the two resonances. **c** shows the magnitude of the transferred magnetisation on spin 2 at a τ_{mix} of 1.2 ms as a function of the resonance offsets of the scalar coupled nuclei, starting with z magnetisation on the first carbon spin at zero mixing time. The corresponding optimised phase-modulation profile of the basic element and the performance characteristics of the symmetry $C7_{40}^{1}$ obtained at a spinning speed of 33.333 kHz employing a resonance offset range of ±5 kHz and an RF field strength of 20 kHz are given in the plots shown in (**d**–**f**). The RF phase values of the first 10 slices of the basic C element are given in the supplementary material

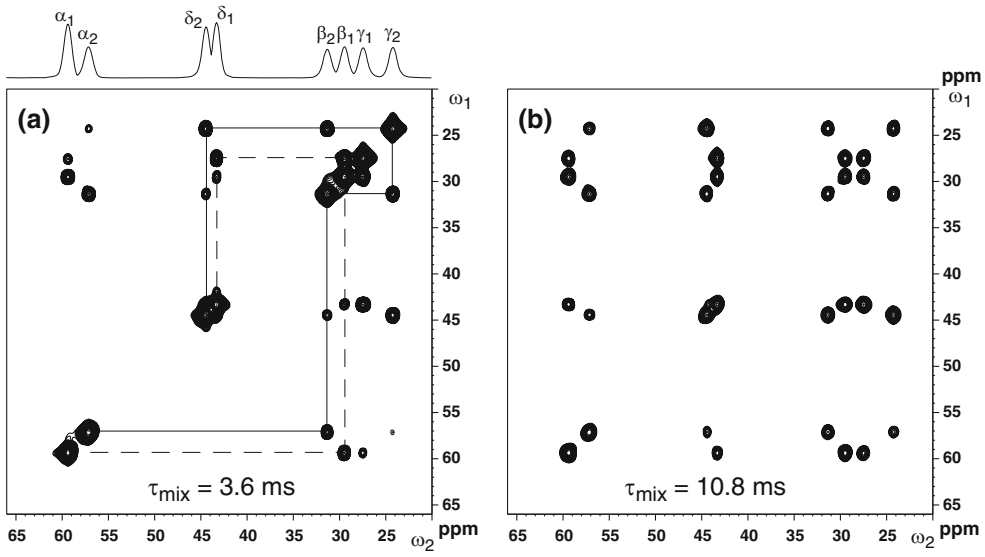

Fig. 4 2D ^{13}C–^{13}C scalar coupling mediated chemical shift correlation spectra (zoomed plot) of L-arginine hydrochloride obtained with a Bruker 500 MHz wide-bore Avance III solid state NMR spectrometer equipped with a 2.5 mm triple resonance probe, at a spinning speed of 33.333 kHz, with ^{13}C RF field strength of 15 kHz during mixing and using mixing times of 3.6 ms (**a**) and 10.8 ms (**b**). The spectra were generated with the $C9^{1}_{120}$ symmetry-based RF pulse scheme, using the basic *C* element with the optimised phase-modulation profile given in Fig. 1, 16 transients per t_1 increment, 64 t_1 increments, spectral width in the indirect dimension of 8,000 Hz, recycle time of 10 s and with the RF carrier kept at 40 ppm

and $C7^{1}_{40}$ symmetries, respectively, at MAS frequencies of 25 and 33.333 kHz. The corresponding optimised phase-modulation profiles of the basic elements and the performance characteristics of the sequences are given in the plots shown in Fig. 3. CSA, scalar and dipolar coupling parameters corresponding to that of the $^{13}C^{\alpha}$ and $^{13}C^{\beta}$ nuclei of alanine were used and the ^{13}C carrier was kept at the middle of the aliphatic spectral region. The simulated magnetisation transfer characteristics indicate the satisfactory performance of the sequences.

The performance characteristics of the symmetry-based sequences reported here were also assessed via experimental measurements and some representative data are given below. The TOBSY spectra of the aliphatic region of arginine shown in Fig. 4a, b were generated at a spinning speed of 33.333 kHz using the $C9^{1}_{120}$ symmetry with the numerically optimised phase-modulated basic element shown in Fig. 1a employing mixing times of 3.6 and 10.8 ms. Direct and relayed cross-peaks of appreciable intensities can be clearly seen in the spectra. Consistent with the results from numerical simulations, it is seen that low-power symmetry-based mixing sequences can be effectively implemented for the study of isotopically labelled biological systems at high MAS frequencies. The experimental performance of the $C9^{1}_{120}$ symmetry with the numerically optimised phase-modulated basic element shown in Fig. 1d was also found to be satisfactory (data not shown). The performances of the

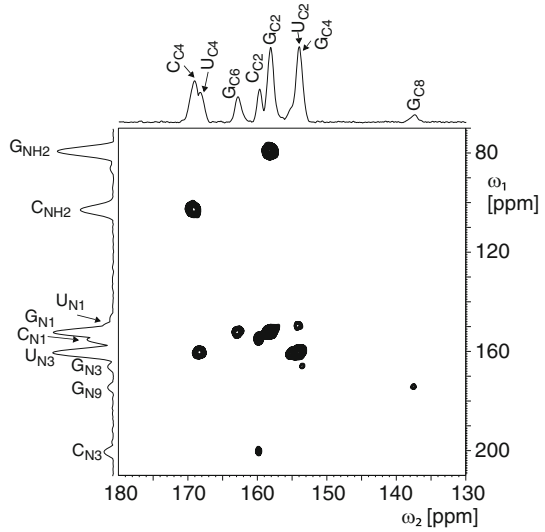

Fig. 5 2D ^{15}N–^{13}C chemical shift correlation spectra (*zoomed plot*) of $(CUG)_{97}$ RNA collected at a spinning speed of 20 kHz via the magnetisation transfer pathway $^{1}H \rightarrow {}^{15}N \rightarrow {}^{13}C$ with a Bruker 750 MHz narrow-bore Avance III solid state NMR spectrometer equipped with a 3.2 mm triple resonance probe. The $R16^{-4,5}_{63}$ symmetry with the corresponding numerically optimised *R* elements given in Fig. 2a1 and b1, a CP contact time of 1.1 ms, a mixing time of 3.15 ms, ^{13}C and ^{15}N RF field strength of 10 kHz, 32 transients per t_1 increment, 64 t_1 increments, spectral width in the indirect dimension of 20,000 Hz and a recycle time of 2.0 s were used, keeping the ^{13}C and ^{15}N RF carriers, respectively, at 161 and 174 ppm

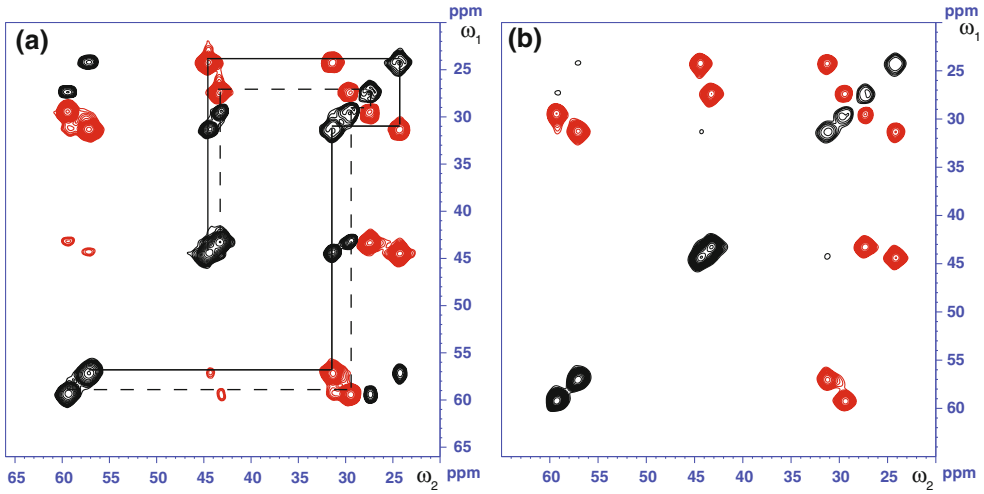

Fig. 6 2D ^{13}C–^{13}C dipolar coupling mediated chemical shift correlation spectra (*zoomed plot*) of L-arginine hydrochloride obtained with a Bruker 500 MHz wide-bore Avance III solid state NMR spectrometer equipped with a 2.5 mm triple resonance probe at spinning speeds of 25 kHz (**a**) and 33.333 kHz (**b**). The spectra were collected with the $C7^{6}_{30}$ symmetry-based RF pulse scheme employing ^{13}C dipolar recoupling RF field strengths of 15 kHz (**a**) and 20 kHz (**b**), mixing times of 1.2 ms (**a**) and 0.9 ms (**b**), 16 transients per t_1 increment, 80 t_1 increments, spectral width in the indirect dimension of 8,000 Hz, recycle time of 10 s and with the RF carrier kept at 40 ppm. The duration of the optimised phase-modulation profile given in Fig. 3a was scaled down to 128.57 μs in acquiring the spectrum 6**b**

dual- channel symmetry-based sequences were assessed via experimental measurements carried out (both at 500 and 750 MHz) on a polycrystalline sample of the CUG triplet repeat expansion RNA $(CUG)_{97}$. Figure 5 shows a representative 2D ^{15}N–^{13}C chemical shift correlation spectrum obtained via longitudinal magnetisation exchange at a spinning speed of 20 kHz using the $R16^{-4,5}_{63}$ symmetry-based double-quantum dipolar recoupling scheme. The spectrum collected via the magnetisation transfer pathway $^{1}H \rightarrow {}^{15}N \rightarrow {}^{13}C$, was obtained employing a CP contact time of 1.1 ms. The cross-peak intensities seen in the heteronuclear correlation spectra are not only related to the efficacy of the dipolar recoupling scheme but also to the starting ^{15}N magnetisation at $\tau_{mix} = 0$. Hence, in addition to $^{15}N \rightarrow {}^{13}C$ crosspeaks arising from nitrogens with directly attached protons, measurable signal intensities are also seen even from ^{15}N nuclei without any attached protons, as indicated. The scalability of the mixing sequences was also tested experimentally. For example, at the spinning speed of 30 kHz, the performance of the $R16^{-5,4}_{49}$ symmetry employing the correspondingly scaled basic R elements (Fig. 2a2, b2) with $^{15}N/^{13}C$ RF field strengths of ~20 kHz was also found to be satisfactory (data not shown). The ^{13}C–^{13}C dipolar correlation spectrum of the aliphatic region of arginine shown in Fig. 6 was generated at a spinning speed of 25 kHz using the $C7^{6}_{30}$ symmetry employing the numerically optimised phase-modulated basic element shown in Fig. 3a and a mixing time of 1.2 ms. Direct and relayed cross-peaks of appreciable intensities can be clearly seen in the spectrum. The performance of this pulse sequence has been found to be satisfactory even at a spinning speed of 33.333 kHz (Fig. 6b). The experimental performance of the $C7^{1}_{40}$ symmetry with the numerically optimised phase-modulated basic element shown in Fig. 3d was also found to be satisfactory at a spinning speed of 33.333 kHz (data not shown). Consistent with the results from numerical simulations, the experimental results presented here demonstrate that low-power symmetry-based mixing sequences can be effectively implemented for the study of isotopically labelled biological systems at high MAS frequencies using symmetries involving the application of basic elements of relatively long duration. Hence, the design of mixing sequences via the symmetry-based approach is neither restricted to broadband mixing nor to moderate MAS frequencies. It is seen that by selecting appropriate symmetries and optimising the RF field modulation profile of the basic elements, it is equally possible to implement both high-power broadband and low-power band-selective mixing sequences at any desired MAS frequency.

Acknowledgments This study has been funded in part by a grant from the Deutsche Forschungsgemeinschaft (GO474/6-1). The FLI is a member of the Science Association'Gottfried Wilhelm Leibniz' (WGL) and is financially supported by the Federal Government of Germany and the State of Thuringia.

References

Bak M, Nielsen NC (1997) REPULSION, a novel approach to efficient powder averaging in solid state NMR. J Magn Reson 125:132–139

Baldus M, Meier BH (1996) Total correlation spectroscopy in the solid state. The use of scalar couplings to determine the through-bond connectivity. J Magn Reson A 121:65–69

Baldus M, Petkova AT, Herzfeld J, Griffin RG (1998) Cross polarization in the tilted frame: assignment and spectral simplification in heteronuclear spin systems. Mol Phys 95:1197–1207

Bennett AE, Rienstra CM, Griffiths JM, Zhen W, Lansbury PT, Griffin RG (1998) Homonuclear radio frequency-driven recoupling in rotating solids. J Chem Phys 108:9463–9479

Brinkmann A, Levitt M (2001) Symmetry principles in the nuclear magnetic resonance of spinning solids: heteronuclear recoupling by generalized Hartmann-Hahn sequences. J Chem Phys 115:357–384

Castellani F, van Rossum BJ, Diehl A, Rehbein K, Oschkinat H (2003) Determination of solid- state NMR structures of proteins by means of three-dimensional 15N–13C–13C dipolar correlation spectroscopy and chemical shift analysis. Biochem 42: 11476–11483

Chen L, Olsen RA, Elliott DW, Boettcher JM, Zhou DH, Reinstra CM, Mueller LJ (2006) Constant-time through-bond 13C correlation spectroscopy for assigning protein resonances with solid state NMR spectroscopy. J Am Chem Soc 128:9992–9993

Chen L, Kaiser JM, Polenova T, Yang J, Reinstra CM, Mueller LJ (2007a) Backbone assignments in solid-state proteins using J-based 3D heteronuclear correlation spectroscopy. J Am Chem Soc 129:10650–10651

Chen L, Kaiser JM, Lai J, Polenova T, Yang J, Reinstra CM, Mueller LJ (2007b) J-based 2D homonuclear and heteronuclear correlation in solid state proteins. Magn Reson Chem 45:S84–S92

Cheng VB, Suzukawa HH, Wolfsberg M (1973) Investigations of a nonrandom numerical method for multidimensional integration. J Chem Phys 59:3992–3999

Detken A, Hardy EH, Ernst M, Kainosho M, Kawakami T, Aimoto S, Meier BH (2001) Methods for sequential resonance assignment in solid, uniformly 13C, 15N labelled peptides: quantification and application to antamanide. J Biomol NMR 20:203–221

Frericks HL, Zhou DH, Yap LL, Gennis RB, Rienstra CM (2006) Magic-angle spinning solid- state NMR of a 144 kDa membrane protein complex: *E.coli* cytochrome bo_3 oxidase. J Biomol NMR 36:55–71

Hansen JO, Kehlet C, Bjerring M, Vosegaard T, Glaser SJ, Khaneja N, Nielsen NC (2007) Optimal control based design of composite dipolar recoupling experiments by analogy to single-spin inversion pulses. Chem Phys Lett 447:154–161

Hardy EH, Detken A, Meier BH (2003) Fast-MAS total through-bond correlation spectroscopy using adiabatic pulses. J Magn Reson 165:208–218

Herbst C (2010) Korrelationen der chemischen Verschiebung an schnell rotierenden biologischen Festkörpern mittels NMR-spectroskopie, Ph.D Thesis, Friedrich-Schiller-University, Jena

Herbst C, Herbst J, Kirschstein A, Leppert J, Ohlenschläger O, Görlach M, Ramachandran R (2009a) Design of high-power, broadband 180° pulses and mixing sequences for fast MAS solid state chemical shift correlation NMR spectroscopy. J Biomol NMR 43:51–61

Herbst C, Herbst J, Kirschstein A, Leppert J, Ohlenschläger O, Görlach M, Ramachandran R (2009b) Recoupling and decoupling of nuclear spin interactions at high MAS frequencies: numerical design of CN_n^v symmetry-based RF pulse schemes. J Biomol NMR 44:175–184

Herbst C, Herbst J, Leppert J, Ohlenschläger O, Görlach M, Ramachandran R (2009c) Numerical design of RN_n^v symmetry-based RF pulse schemes for recoupling and decoupling of nuclear spin interactions at high MAS frequencies. J Biomol NMR 44:235–244

Herbst C, Herbst J, Leppert J, Ohlenschläger O, Görlach M, Ramachandran R (2010) Broadband 15N–13C dipolar recoupling via symmetry-based RF pulse schemes at high MAS frequencies. J Biomol NMR 47:7–17

Hong M (1999) Resonance assignment of 13C/15N labeled solid proteins by two- and three- dimensional magic-angle-spinning NMR. J Biomol NMR 15:1–14

Kehlet C, Bjerring M, Sivertsen AC, Kristensen T, Enghild JJ, Glaser SJ, Khaneja N, Nielsen NC (2007) Optimal control based NCO and NCA experiments for spectral assignment in biological solid-state NMR spectroscopy. J Magn Reson 188:216–230

Levitt MH (2002) Symmetry-based pulse sequences in magic-angle spinning solid-state NMR. In: Grant DM, Harris RK (eds) Encyclopedia of nuclear magnetic resonance. John Wiley, Chichester

Nielsen AB, Bjerring M, Nielsen JT, Nielsen NC (2009) Symmetry-based dipolar recoupling by optimal control: band-selective experiments for assignment of solid-state NMR spectra of proteins. J Chem Phys 131:025101

Nielsen AB, Jain SK, Nielsen NC (2011) Low-power homonuclear dipolar recoupling using supercycled symmetry-based and exponentially-modulated pulse sequences. Chem Phys Lett 503: 310–315

Pauli J, Baldus M, van Rossum B, de Groot H, Oschkinat H (2001) Backbone and side-chain 13C and 15N signal assignments of the α-spectrin SH3 domain by magic angle spinning solid-state NMR at 17.6 Tesla. ChemBioChem 2:272–281

Riedel K, Leppert J, Ohlenschläger O, Görlach M, Ramachandran R (2005) TEDOR with adiabatic inversion pulses: resonance assignments of 13C/15N labelled RNAs. J Biomol NMR 31: 49–57

Riedel K, Herbst C, Häfner S, Leppert J, Ohlenschläger O, Swanson MS, Görlach M, Ramachandran R (2006) Constraints on the structure of (CUG)97 RNA from magic-angle- spinning solid-state NMR spectroscopy. Angew Chem Int Ed 45:5620–5623

Rienstra CM, Hohwy M, Hong M, Griffin R (2000) 2D and 3D 15N–13C–13C Chemical Shift Correlation Spectroscopy of Solids: Assignment of MAS Spectra of Peptides. J Am Chem Soc 122: 10979–10990

Siemer AB, Ritter C, Steinmetz MO, Ernst M, Riek R, Meier BH (2006) 13C, 15N Resonance assignment of parts of the HET-s prion protein in its amyloid form. J Biomol NMR 34:75–87

Sun BQ, Rienstra CM, Costa PR, Williamson JR, Griffin RG (1997) 3D 15N–13C–13C chemical shift correlation spectroscopy in rotating solids. J Am Chem Soc 119:8540–8546

van Rossum BJ, Castellani F, Pauli J, Rehbein K, Hollander J, de Groot HJM, Oschkinat H (2003) Assignment of amide proton signals by combined evaluation of HN, NN and HNCA MAS-NMR correlation spectra. J Biomol NMR 25:217–223

Veshtort M, Griffin RG (2006) SPINEVOLUTION: a powerful tool for the simulation of solid and liquid state NMR experiments. J Magn Reson 178:248–282

Zhou DH, Shah G, Cormos M, Franks WT, Mullen C, Sandoz D, Rienstra CM (2007a) Proton—detected solid-state NMR spectroscopy of fully protonated proteins at 40 kHz magic-angle spinning. J Am Chem Soc 129:11791–11801

Zhou DH, Shea JJ, Nieuwkoop AJ, Franks WT, Wylie BJ, Mullen C, Sandoz D, Rienstra CM (2007b) Solid-state protein-structure determination with proton-detected triple-resonance 3D magic-angle-spinning NMR spectroscopy. Angew Chem Int Ed 46: 8380–8383